Check for updates

Insulin amyloid fibril formation reduction by tripeptide stereoisomers†

Beatrice Rosetti, [a] Slavko Kralj, [b,c] Erica Scarel, [a] Simone Adorinni, [a] Barbara Rossi, [d] Attilio V. Vargiu, [e] Ana M. Garcia *[f] and Silvia Marchesan *[a]

Insulin fibrillation is a problem for diabetic patients that can occur during storage and transport, as well as at the subcutaneous injection site, with loss of bioactivity, inflammation, and various adverse effects. Tripeptides are ideal additives to stabilise insulin formulations, thanks to their low cost of production and inherent cytocompatibility. In this work, we analysed the ability of eight tripeptide stereoisomers to inhibit the fibrillation of human insulin *in vitro*. The sequences contain proline as β-breaker and Phe−Phe as binding motif for the amyloid-prone aromatic triplet found in insulin. Experimental data based on spectroscopy, fluorescence, microscopy, and calorimetric techniques reveal that one stereoisomer is a more effective inhibitor than the others, and cell live/dead assays confirmed its high cytocompatibility. Importantly, *in silico* data revealed the key regions of insulin engaged in the interaction with this tripeptide, rationalising the molecular mechanism behind insulin fibril formation reduction.

Introduction

The pathological fibrillation of amyloids is an unsolved challenge in medicine. At least 50 proteins or peptides have been found to aggregate into amyloid structures with various adverse effects on human health. The most widely known amyloidoses are linked to neurodegenerative processes, such as the Alzheimer's, Huntington's, and Parkinson's diseases.[1] However, many more exist, and amyloids' new roles are continuously being found, for instance affecting the heart,[2] the kidney,[3] or the gut.[4]

The tendency of these proteins or peptides to fibrillate is not directly associated to their primary amino acidic sequence, as it is a general feature of a wide number of polypeptides under appropriate conditions.[5–9] However, those polypeptides normally share common physico-chemical properties, such as high hydrophobicity with low net charge, and high propensity

to convert from an α-helix towards a β-sheet. Amyloid aggregation typically involves protein unfolding or re-folding into a non-functional form, which then can stack to give rise to the cross-β hallmark found in fibrils.[10] In fact, in neurodegenerative diseases, soluble oligomers demonstrated higher toxicity than mature fibrils, showing the importance to tackle the early stages of aggregation.[11,12] As a result of fibrillation, physiological disfunctions occur that can lead to a cascade of adverse effects, especially when the protein or peptide is a hormone or it is involved in its transport.[13–16]

In particular, insulin fibrillation can cause cytotoxicity and inflammation,[17] which can be exacerbated by its ability to promote fibrillation of other proteins, such as amylin.[18] Besides, an increased risk of developing neurodegenerative syndromes has been linked to insulin dysfunction.[19] Insulin fibrillation is a problem of particular relevance for diabetic patients. It can occur at the site of subcutaneous injection, or during transport and storage, being promoted by several factors, such as agitation, high ionic strength, high concentration, and low pH.[20] Therefore, there is large scope for the identification of simple biomolecules that could serve as functional additives to stabilise insulin formulations. Several peptides have been studied for their ability to inhibit insulin fibrillation, with their design being typically based on insulin-binding sequences, for instance those found in the insulin receptor or in insulin itself.[21]

In this regard, peptides as short as two-to-three amino acids are particularly advantageous for their low-cost of production and generally high cytocompatibility, as demonstrated by their wide use in supplements, nutraceuticals, and medic-

[a] Chemical Pharmaceutical Science Department, University of Trieste, 34127 Trieste, Italy. E-mail: smarchesan@units.it

[b] Materials Synthesis Department, Jožef Stefan, Institute, 1000 Ljubljana, Slovenia

[c] Department of Pharmaceutical Technology, Faculty of Pharmacy, University of Ljubljana, 1000 Ljubljana, Slovenia

[d] Elettra Sincrotrone Trieste, Strada Statale 14 - km 163,5 Basovizza, 34149 Trieste, Italy

[e] Physics Department, University of Cagliari, 09042 Monserrato, Cagliari, Italy

[f] Facultad de Ciencias y Tecnologías Químicas, Instituto Regional de Investigación Científica Aplicada (IRICA), Universidad de Castilla-La Mancha, 13071 Ciudad Real, Spain. E-mail: anam.garcia@uclm.es

†Electronic supplementary information (ESI) available: TEM micrographs and UVRR spectra. See DOI: https://doi.org/10.1039/d4nr00693c

inal products.[22] The di- and tri-peptides used to inhibit insulin fibrillation were based on the Phe–Phe motif,[23] which has a strong tendency to fibrillate and is found in insulin itself,[24] coupled with a ferrocenyl unit (Fc).[25,26] Best results were obtained with the tripeptides Fc–Phe–Phe–Phe and Fc–Phe–Phe–Tyr, which can be rationalised with the finding that tripeptides have the ideal number of non-hydrogen atoms for maximal efficacy of binding with receptors, hence for bioactivity.[27] However, in those studies the effect of amino acid stereoconfiguration was not evaluated. Recently, we reported the detailed investigation of the supramolecular behaviour of the complete series of Pro–Phe–Phe stereoisomers, which contain proline as β-breaker and Phe–Phe as anchoring unit to inhibit amyloid fibrillation.[28] In particular, L-Pro–D-Phe–L-Phe revealed to be the most effective inhibitor *in vitro*, with excellent cytocompatibility and resistance against enzyme-mediated hydrolysis.[28] Therefore, in this study, we focussed on insulin as a target to assess whether their inhibitory activity can be extended to other amyloids, and whether appropriate choice of stereoconfiguration can enable target selectivity.

Results and discussion

Tripeptide series preparation

The eight Pro–Phe–Phe stereoisomers (Scheme 1) were prepared by solid-phase peptide synthesis using Fmoc-protection strategy and standard protocols, as previously reported.[28] Their purification by reverse-phase high-performance liquid chromatography (RP-HPLC) led to pure peptides, as confirmed by LC-MS analyses, ^{1}H- and ^{13}C-NMR data, which were in agreement with the literature.[28]

Insulin fibrillation inhibition

Insulin is a heterodimeric α-helical protein, which is composed of two chains, A and B. At physiological pH, insulin is in a stable, zinc-bound hexameric form (Fig. 1a), while the bioactive monomer can undergo partial unfolding to expose aggregation-prone hydrophobic surfaces (Fig. 1b).[20] Among these, the segment Leu–Val–Glu–Ala–Leu–Tyr–Leu (LVEALYL in Fig. 1b) of chain B plays a key role in insulin fibrillation. X-ray diffraction data revealed that it is central to the cross-β spine of insulin fibrils, as two adjacent LVEALYL segments interlock in a dry steric zipper, as a result of their conversion from the native α-helical conformation into extended β-strands.[29] Another hydrophobic segment is the "aromatic triplet" Phe–Phe–Tyr (FFY in Fig. 1b) that is found near the C-terminus of chain B. This conserved motif creates an extended apolar surface, and it can establish intermolecular aromatic interactions with other triplets of insulin molecules.[24]

There are several protocols to reproduce *in vitro* insulin fibrillation, which is not trivial and it is influenced by a number of factors, such as temperature, agitation, ionic strength and insulin concentration.[30] Under physiological conditions, insulin fibrillation *in vitro* can take several days, there-
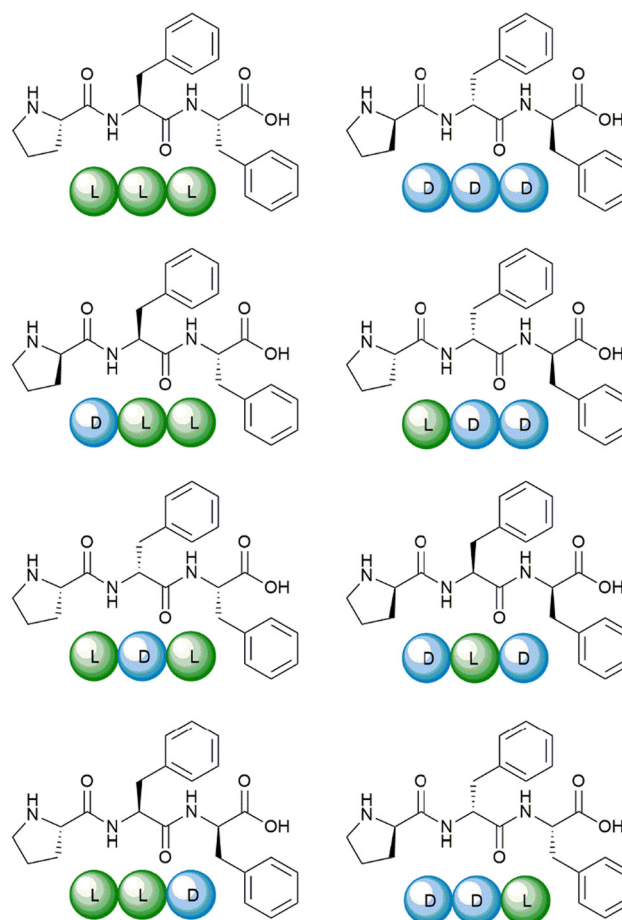
Scheme 1 The eight Pro–Phe–Phe stereoisomers synthesized and studied as inhibitors of insulin fibrillation.

fore acidic conditions are typically used to conveniently reduce the lag time.[25,26,31–34] In particular, for this study we chose the use of NaCl, strong agitation, 37 °C and a pH 1.6 that are ideal experimental conditions to reduce variability amongst insulin concentration values and reduce the fibrillation lag time.[35]

Thioflavin-T fluorescence assay. Thioflavin-T (ThT) is a well-known dye that is widely used as amyloid marker thanks to its ability to bind to the surface of fibrils, thus yielding fluorescence as a consequence of the impeded rotation of a chemical bond connecting its two aromatic core units.[36] This assay has been successfully applied to study the fibrillation of insulin too, although experimental conditions can lead to varying degrees of fluorescence, which is further affected by insulin conformers' differing ability to bind to ThT.[37]

Indeed, initial attempts to quantitatively monitor the kinetics of fibrillation led to reproducibility issues especially over the first hours, therefore we opted for 48 h end-points instead. In this manner, it was possible to note that the most effective inhibitor was the homochiral L-Pro–L-Phe–L-Phe, followed by D-Pro–L-Phe–D-Phe and L-Pro–L-Phe–D-Phe stereoisomers (Fig. 1c). Surprisingly, among the worst performers with negligible inhibitory activity, there was L-Pro–D-Phe–L-Phe that was
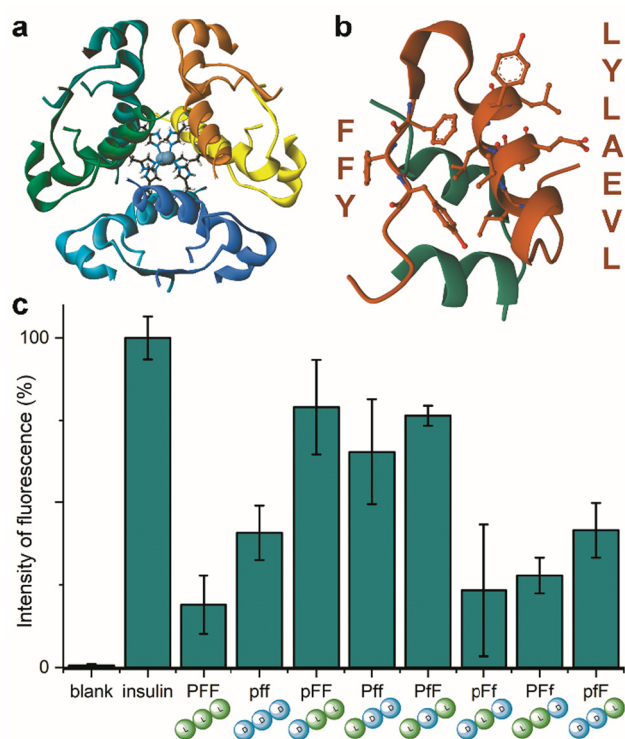
["

Fig. 3 (a) CD spectra of insulin before (dotted line) and after 48 h of fibrillation (solid line). (b) CD spectra of insulin fibrils treated with each one of the three Pro–Phe–Phe inhibitors (ʟ–ʟ–ʟ, orange; ᴅ–ʟ–ᴅ blue; ʟ–ʟ–ᴅ green) or untreated (black) after 48 h. (c) Dose–response ThT assay with increasing concentrations of ʟ-Pro–ʟ-Phe–ʟ-Phe. (d) DSC data of insulin fibrils (black) and treated with ʟ-Pro–ʟ-Phe–ʟ-Phe (orange).

equivalent of Pro-Phe-Phe relative to insulin, which in the case of the test corresponded to 14 μM. An excess of inhibitor led to a maximum reduction of fibrillation by approximately 75%, in agreement with the ThT data shown in Fig. 1.
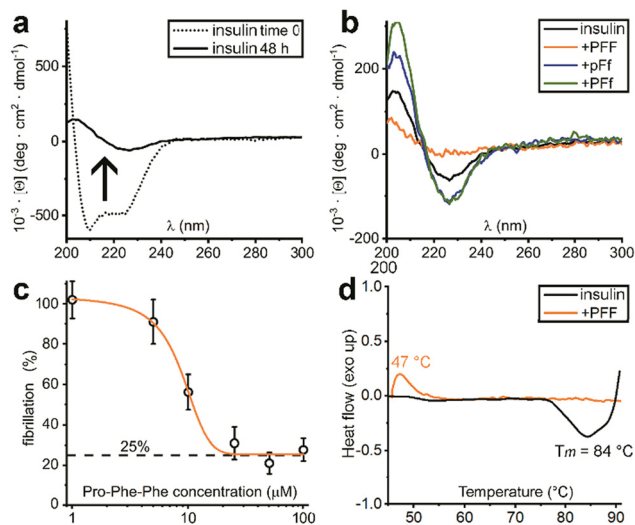
Differential scanning calorimetry (DSC). DSC analyses performed on insulin fibrils revealed their typical high thermal stability, with the endothermic peak at 84 °C (T_{onset} = 76 °C) due to their denaturation, in agreement with the literature.[38,39] Absence of both exothermic signals associated with unfolding and aggregation of insulin suggested that the polypeptide was completely fibrillated after 48 hours. Presence of ʟ-homochiral Pro–Phe–Phe resulted in the disappearance of the endothermic peak, with the concomitant appearance of the characteristic exothermic signal of native insulin monomers, with a maximum at 47 °C.[40,41] The exothermic signal is associated with a volume expansion of the polypeptide as its tertiary contacts are loosened to yield a "molten-globule" form.[42] Overall, the calorimetric analysis confirmed the inhibitory effect of ʟ-Pro–ʟ-Phe–ʟ-Phe on insulin fibrillation.

UV resonance Raman spectroscopy (UVRR)

UVRR has been demonstrated to be a powerful tool for probing amyloid fibril structures in proteins at all stages of aggregation.[43–46] With respect to conventional visible Raman technique, UV enhancement provides a significant increment of the detection limit, being particularly useful for investigating diluted samples. Additionally, the use of different excitation wavelengths allows for a selective resonance enhancement of specific portions in proteins. In particular, the use of an excitation wavelength at 226 nm is convenient to probe the aromatic signals of Phe and Tyr residues, thanks to the close resonance of this excitation energy with their electronic

transitions.[47,48] The consequent strong enhancement of the UV Raman cross-section of some vibrational modes attributed to Phe and Tyr makes these signals the predominant ones in the UVRR spectra, as confirmed by analysis of amino acid precursors devoid of the amide bond that is normally present in visible Raman spectra.[49]

The UVRR spectra showed that fibrillation markedly reduced the Raman signals of Phe and Tyr at about 1610 cm^{-1} and 1180 cm^{-1} in insulin, which were partially restored in the presence of ʟ-Pro–ʟ-Phe–ʟ-Phe (Fig. 4a). This is evident by looking at the difference spectra (DUVRR, Fig. 4b), which clearly display the effect of PFF to partially inhibit the fibrillation of insulin. The decrease in the intensity of aromatic bands in the DUVRR was observed during insulin aggregation,[43,44,46] suggesting that the local environment of these amino acids is changed upon fibrillation. In particular, the strong reduction of the Raman signal at 1610 cm^{-1} could indicate that Tyr residues are in a more hydrophobic environment than in the native protein.[44]

Instead, in the presence of the tripeptide, the signal intensity is mostly, but not completely, restored, in agreement with the ThT data. Therefore, UVRR data further supported the bioactivity of the tripeptide in markedly reducing fibrillation of insulin.

Insulin-tripeptide interactions

The interaction between insulin and ʟ-homochiral Pro–Phe–Phe (PFF) or ʟ-Pro–ᴅ-Phe–ʟ-Phe (hereafter PfF) was studied by means of all-atom MD simulations. Studies were performed at pH 1.6, closer to the conditions of the experiments, and at
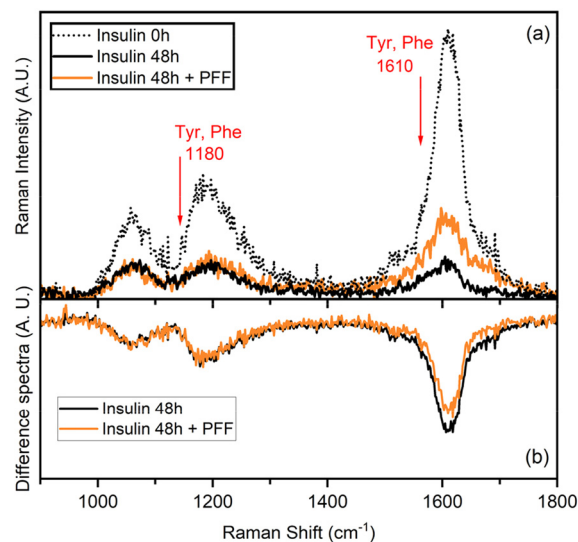
Fig. 4 (a) Raman spectra of insulin in the native form (dotted black line) and after 48 h of fibrillation (black line) either alone or in the presence of ʟ-Pro–ʟ-Phe–ʟ-Phe (PFF, orange line). The spectra have been subtracted by the spectral contribution of the solvent and solvent + PFF. (b) Difference spectra [insulin 48 h − insulin 0 h] and [(insulin 48 h + PFF) − insulin 0 h] highlighting that the local environment of Tyr residues changes in the presence or absence of PFF.

physiological pH (7.4). Each amino acid was assigned the most likely protonation state at the corresponding pH values. In both cases, one protein and ten peptides (1 : 10 ratio) were simulated in 0.1 M NaCl water solution at room temperature and pressure. At pH 1.6, MD simulations identified long-lasting interactions formed by one or more homochiral peptides with both the "aromatic triplet" FFY sequence located at the insulin C-terminus and the hydrophobic LVEALYL segment, which is notoriously prone to fibrillation. Examples of molecular arrangements establishing these interactions are reported in Fig. 5 (see also ESI, section S9†). In contrast, not more than one single heterochiral PfF peptide was able to establish stable interactions with the LVEALYL segment in four independent MD simulations (Fig. 5 and ESI section S9†). In addition, the interactions between insulin and the homochiral PFF peptides have a longer lifetime than those established with the heterochiral PfF (see the captions of Fig. 5 and ESI section S9†). A similar situation is seen at pH 7.4, although in this case also PfF establishes interactions with the FFY motif, while the tripeptide-insulin interactions remain stronger for homochiral PFF.

From the MD simulations, it is evident that both tripeptide stereoisomers exploit multiple interaction patterns to bind insulin (see ESI section S9†). In most cases, tripeptide Phe residues interact directly with the sidechains of the hydrophobic FFY triplet and LVEALYL stretch. However, in several

dynamics, Pro is also involved in direct contacts with insulin, and one case (*i.e.*, PFF at pH 1.6, replica 4) there is a strong interaction between the terminal carboxyl group and the insulin backbone.

Overall, these results clearly indicate that regions of the insulin polypeptide involved in the early stages of fibrillation have a strong affinity to homochiral PFF, pointing to a clear putative mechanism of inhibition. The lower inhibitory activity of heterochiral PfF can be partly explained by the different
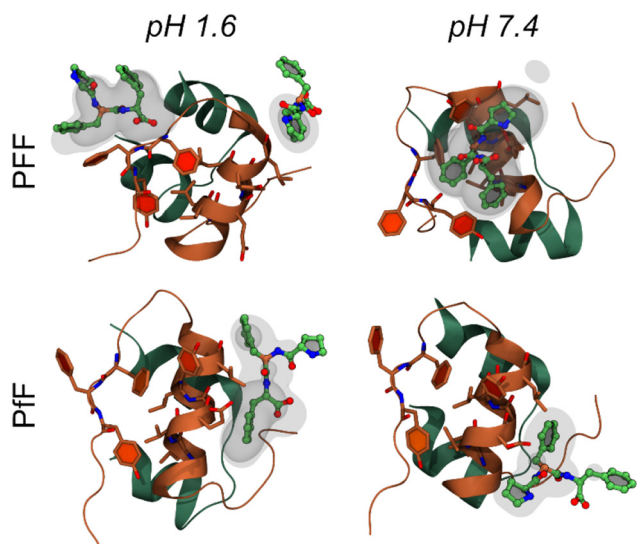
Fig. 5 Molecular interactions between the insulin monomer and PFF (first row) or PfF (second row) stereoisomers. Reported are four examples of highly sampled conformations at pH 1.6 (left column) and pH 7.4 (right), taken from the MD simulations associated to the largest density values calculated among all replicas for each system (form upper-left to bottom-right: 16.8, 11.5, 6.4, and 9.1 respectively, see Methods and ESI section S9†). Insulin is coloured as in Fig. 1b, while peptides are coloured by atomic element (C, O, N in green, red, and blue respectively). Transparent and semi-transparent surfaces represent isosurfaces corresponding respectively to density values 2 and 3 times higher than the value of water at standard conditions.
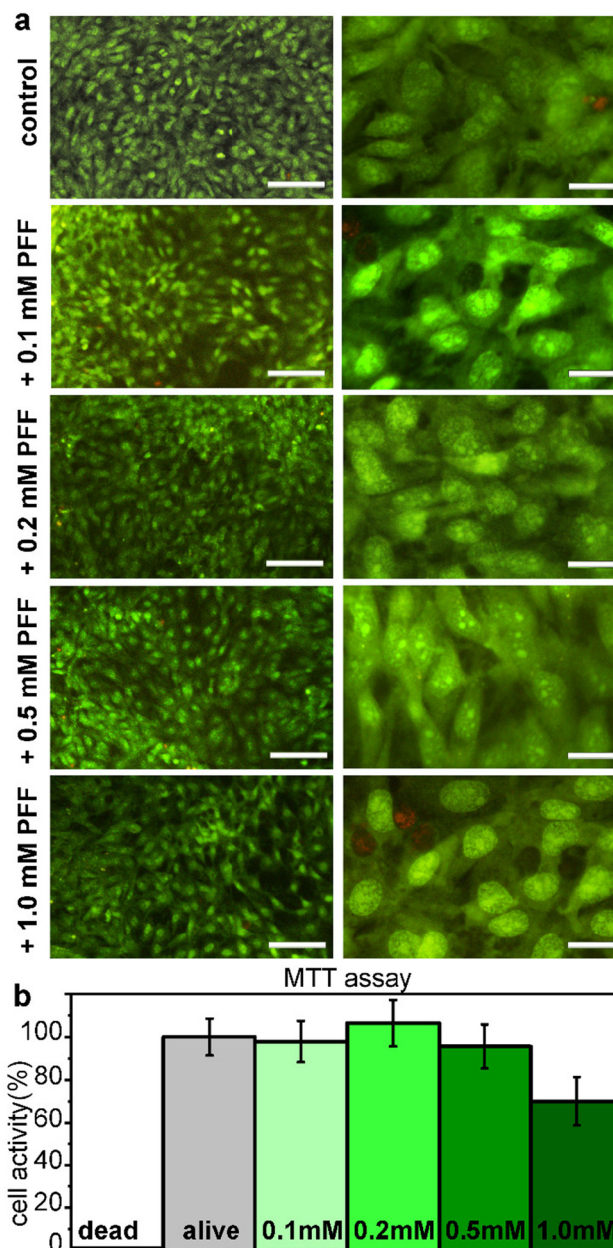
Fig. 6 (a) Microscopy images at low (10×, left panels) or high (40×, right panels) magnification for the live (green)/dead (red) assay for L-Pro−L-Phe−L-Phe on fibroblast cell culture. Scalebars = 100 μm (left panels) and 20 μm (right panels). (b) MTT assay after 24 h exposure to L-Pro−L-Phe−L-Phe at various concentrations.

affinity of this tripeptide towards the protein, although further investigations are required to clearly identify all the molecular determinants behind the peculiar behaviour of the homochiral stereoisomer.

Cytocompatibility of Pro–Phe–Phe

Cytocompatibility of L-Pro–L-Phe–L-Phe was tested *in vitro* on fibroblast cell culture with live/dead and metabolic assays (Fig. 6). No significant difference between the untreated and treated samples was found either in the number of cells, or in their viability or morphology, for all the tested tripeptide concentrations up to 1 mM (Fig. 6a). Similarly, the metabolic MTT assay showed insignificant differences in metabolic activity between untreated and treated fibroblast cells, upon exposure for 24 hours to L-Pro–L-Phe–L-Phe up to 0.5 mM. Metabolic activity was reduced to 70% at the highest concentration of 1 mM, which is remarkably high (Fig. 6b). Overall, these data indicate a promising profile for the tripeptide in terms of cytocompatibility.

Experimental

Materials and methods

Recombinant human insulin produced in yeast (Roche) was purchased from Merck. Fmoc-amino acids, 2-chlorotrityl resin, and coupling agents were obtained from GL Biochem (Shanghai) Ltd. All other reagents and solvents were acquired at analytical grade from Merck. An in-line Millipore RiOs/ Origin system provided high-purity Milli-Q-water with resistivity >18 MΩ cm. ^{1}H-NMR and ^{13}C-NMR spectra were recorded on a Varian Innova at 400 MHz with chemical shift reported as ppm (with tetramethylsilane as internal standard).

An Agilent 6120 LC-MS system was used for ESI-MS spectra. Peptide synthesis, purification, and characterisation, as well as DSC measurements, MTT and live/dead cell assays were carried out as previously described.[28]

ThT assay for insulin fibrillation inhibition

Eppendorf tubes were prepared containing a stock solution of insulin at 172 μM (NaCl 0.1 M and HCl 25 mM, pH 1.6). For the fibrillation inhibition test, insulin stock solutions were transferred to another Eppendorf tube and diluted to 14.3 μM (with NaCl 0.1 M and HCl 25 mM, pH 1.6, 351 μL), to which 8.6 μL of dimethylsulfoxide (DMSO) without or with the tripeptides were added (final concentration 286.6 μM) with a total volume of 300 μL per sample. The tripeptide/insulin molar ratio 20 : 1 was chosen for the initial screenings. Samples were incubated in a thermoblock for the fibrillation process for 48 hours at 980 rpm and 37 °C. Fluorescence emission was measured in triplicate on two independent experiments using a TECAN Infinite M1000 PRO plate reader instrument, selecting an excitation wavelength of 446 nm and an emission wavelength of 490 nm, with a bandwidth of 20 nm. All the samples (50 μL) were added to the wells of Corning 96 flat- and transparent-bottom black polystyrene plates. Thioflavin-T was dis-

solved separately in a 50 mM glycine-NaOH buffer at pH 6.5 and filtered (0.2 μm). The concentration of Thioflavin-T was calculated with the absorbance measurement (ε = 36 000 cm^{-1}, Abs ≈ 0.7, ~21 μM). 150 μl of ThT solution were added on top of samples in the 96-well plate. After 15 minutes, fluorescence was recorded using the parameters indicated above. Average values and standard deviations (n = 6) are plotted. For the dose–response assay, the same procedure was applied using different concentrations of Pro–Phe–Phe.

Transmission electron microscopy (TEM)

Solutions of insulin at 172 μM (NaCl 0.1 M and HCl 25 mM, pH 1.6) with or without the tripeptides (1.7 mM) were prepared in Eppendorf tubes and incubated in a thermoblock at 980 rpm and 37 °C for 48 hours. Copper-lacey carbon film grids were exposed under UV in a UV-Ozone cleaner (UV-Ozone Procleaner Plus) for 5 minutes to increase their surface hydrophilicity. Samples were then immediately deposited on the grids, dried at room temperature and stained with uranyl acetate. TEM micrographs were acquired on a Jeol JEM 2100 instrument at 100 kV. Fibril diameters were measured using ImageJ.

Circular dichroism

Solutions of insulin at 172 μM (NaCl 0.1 M and HCl 25 mM, pH 1.6) without or with the tripeptides (344 μM), were prepared in Eppendorf tubes. Samples were incubated in a thermoblock at 980 rpm and 37 °C for 48 hours. Samples were then transferred into 0.1 mm quartz cuvettes and measured in a Jasco J815 spectropolarimeter, with one accumulation, D.I.T. 2 s, bandwidth of 1 nm, data pitch 0.5 nm, scanrate 50 nm min^{-1} and a range of wavelength from 200 to 300 nm. Spectra were averaged (n = 10) and plotted.

UV resonance Raman spectroscopy (UVRR)

UVRR spectra were collected on the BL10.2-IUVS beamline of Elettra Synchrotron Trieste (Italy)[49] using an excitation wavelength at 226 nm provided by the synchrotron radiation (SR). The excitation energy was set by regulating the undulator gap aperture and monochromatizing the incoming SR light with a Czerny-Turner monochromator (Acton SP2750, Princeton Instruments, Acton, MA, USA) equipped with a holographic grating with 3600 groves per mm. All UVRR spectra were recorded in back-scattered geometry by using a single pass of a Czerny-Turner spectrometer (Trivista 557, Princeton Instruments, 750 mm of focal length) equipped with a holographic grating at 1800 grooves per mm. The spectral resolution was set at 1.6 cm^{-1} per pixel. The calibration of the spectrometer was standardized using cyclohexane (spectroscopic grade, Sigma Aldrich). Any possible photodamage effect due to prolonged exposure of the sample to UV radiation (the maximum beam power measured on the sample was tens of μW) was avoided by continuously spinning the sample cell during measurements. All samples were freshly dissolved in buffer for assembly and placed in quartz cuvettes for UVRR measurements. The temperature was set at 298 K. Samples

were prepared as described above, with insulin at 172 µM (NaCl 0.1 mM, HCl 25 mM, pH 1.6) at time 0 (native form) and after fibrillation at 37 °C and 980 rpm for 48 hours without or with L-Pro–L-Phe–L-Phe (1.7 mM). Peptide controls did not contain insulin.

Molecular modelling

All-atom MD simulations and analyses were performed with the AMBER20 and AmberTools21 software packages.[50] The structure of insulin was taken from the PDB databank (PDB entry 3I40,[51] while the conformation of PFF was generated using the sequence command of the *tleap* module and further optimising the structure. The conformation of PfF was generated from that of PFF by inverting the chirality if the central amino acid using VMD1.9.3[52] and further optimising the structure with *tleap*. Next, 10 peptides were randomly placed around the protein and the system was solvated with 0.1 M NaCl water solution (OPC model for water). Two conditions, corresponding to the most likely protonation state of each amino acid at pH 1.6 and 7.4, were used to mimic experimental and physiological conditions. In the first case, both Asp and Glu sidechain carboxyl group were protonated at one oxygen, and the His were also protonated on both nitrogens. Finally, all C-termini (protein and tripeptides) were protonated.

The ff19SB force field was used for the peptides and the proteins.[53] All the simulations were performed as follows. First, three consecutive restrained structural optimizations (up to 25 000 steps) were performed in the presence of harmonic restraints (k = 1 kcal mol^{-1} Å^{-1}) applied to: (a) all non-hydrogenous atoms of the system; (b) backbone atoms; (c) C$_\alpha$ atoms. Reference structures at steps (b) and (c) were the final ones from the previous step. Next, up to 50 000 cycles of unrestrained optimization were performed. Each system was then heated to 298.15 K in 1 ns *via* constant-pressure-temperature (NTP) MD simulations (using the isotropic Berendsen barostat and the Langevin thermostat) followed by an equilibration phase of 10 ns. Starting from the equilibrated structure, four MD simulation replicas, each of 0.5 µs in length, were performed for each system using a time step of 2 fs. Periodic boundary conditions were employed, and electrostatic interactions were estimated using the Particle Mesh Ewald scheme with a cutoff of 9.0 Å for the short-range evaluation in direct space and for Lennard–Jones interactions (with a continuum model correction for energy and pressure).

Spatial density of the tripeptides around insulin were calculated over the production trajectory with the *grid* command of the cpptraj tool of AMBER20, using a spacing of 0.5 Å in each direction. Figures were prepared with VMD1.9.3.[52]

Conclusions

In conclusion, this work analysed the complete stereoisomer series of eight Pro–Phe–Phe tripeptides as inhibitors for human insulin fibrillation. The L-homochiral compound was

the best inhibitor leading to a reduction of fibrillation *in vitro* by 75% when an excess peptide was used, and inhibiting 50% of the fibrillation when 1 molar equivalent relative to insulin was present. The inhibitory activity was confirmed by a series of spectroscopic, microscopic, and calorimetric techniques, and lack of cytotoxicity was evident with live/dead assays on fibroblast cells *in vitro*, confirming the potential for this compound as additive to stabilise insulin formulations. *In silico* data confirmed that the design, which was based on the combination of Pro as a β-breaker, and Phe-Phe as a binding motif for the "aromatic triplet" at the insulin C-terminus was successful. Importantly, another key interaction was found with the hydrophobic LVEALYL segment, which is notoriously prone to fibrillation. Considering the high potential for such low-cost and biocompatible short peptides as additives for therapeutic formulations,[54] this work paves the way to further developments in this exciting research area.

Author contributions

B. R., S. K., E. S., S. A., A. V. V., A. M. G. – investigation; S. A., B. R., A. M. G., S. M. – supervision; B. R., A. V. V., A. M. G., S. M. – visualization; A. M. G., S. M. – conceptualization; A. M. G. – initial draft writing; all authors – writing and editing.

Conflicts of interest

There are no conflicts to declare.

Acknowledgements

References

1 M. G. Iadanza, M. P. Jackson, E. W. Hewitt, N. A. Ranson and S. E. Radford, *Nat. Rev. Mol. Cell Biol.*, 2018, **19**, 755–773.

2 K. Sud, N. Narula, E. Aikawa, E. Arbustini, P. Pibarot, G. Merlini, R. S. Rosenson, S. V. Seshan, E. Argulian,

A. Ahmadi, F. Zhou, A. L. Moreira, N. Côté, S. Tsimikas, V. Fuster, S. Gandy, R. O. Bonow, O. Gursky and J. Narula, *Nat. Rev. Cardiol.*, 2023, **20**, 418–428.

3 S. Karam, M. Haidous, V. Royal and N. Leung, *Kidney Int.*, 2023, **103**, 473–484.

4 M. G. Herrera and V. I. Dodero, *Biophys. Rev.*, 2021, **13**, 1147–1154.

5 F. Chiti, P. Webster, N. Taddei, A. Clark, M. Stefani, G. Ramponi and C. M. Dobson, *Proc. Natl. Acad. Sci. U. S. A.*, 1999, **96**, 3590–3594.

6 E. Gazit, *Angew. Chem., Int. Ed.*, 2002, **41**, 257–259.

7 F. Hane, *FEBS Lett.*, 2013, **587**, 3617–3619.

8 P. C. Ke, R. Zhou, L. C. Serpell, R. Riek, T. P. J. Knowles, H. A. Lashuel, E. Gazit, I. W. Hamley, T. P. Davis, M. Fändrich, D. E. Otzen, M. R. Chapman, C. M. Dobson, D. S. Eisenberg and R. Mezzenga, *Chem. Soc. Rev.*, 2020, **49**, 5473–5509.

9 A. M. Garcia, C. Giorgiutti, Y. El Khoury, V. Bauer, C. Spiegelhalter, E. Leize-Wagner, P. Hellwig, N. Potier and V. Torbeev, *Chem. – Eur. J.*, 2020, **26**, 9889–9899.

10 F. Chiti, M. Stefani, N. Taddei, G. Ramponi and C. M. Dobson, *Nature*, 2003, **424**, 805–808.

11 S. Ghosh, R. Ali and S. Verma, *Int. J. Biol. Macromol.*, 2023, **239**, 124231.

12 K. Kulenkampff, A. M. Wolf Perez, P. Sormanni, J. Habchi and M. Vendruscolo, *Nat. Rev. Chem.*, 2021, **5**, 277–294.

13 M. Spiess, N. Beuret, C. Prescianotto Baschong and J. Rutishauser, in *Vitamins and Hormones*, ed. G. Litwack, Academic Press, 2020, vol. 113, pp. 55–77.

14 S. Sen, R. Ali, A. Onkar, S. Ganesh and S. Verma, *ChemBioChem*, 2022, **23**, e202100678.

15 F. Manganelli, G. M. Fabrizi, M. Luigetti, P. Mandich, A. Mazzeo and D. Pareyson, *Neurol. Sci.*, 2022, **43**, 595–604.

16 A. K. Bishoyi, P. H. Roham, K. Rachineni, S. Save, M. A. Hazari, S. Sharma and A. Kumar, *Biol. Chem.*, 2021, **402**, 133–153.

17 B. E. Lewis, A. Mulka, L. Mao, R. Sharafieh, Y. Qiao, S. Kesserwan, R. Wu, D. Kreutzer and U. Klueh, *J. Diabetes Sci. Technol.*, 2023, **17**, 163–171.

18 W. Cui, J.-W. Ma, P. Lei, W.-H. Wu, Y.-P. Yu, Y. Xiang, A.-J. Tong, Y.-F. Zhao and Y.-M. Li, *FEBS J.*, 2009, **276**, 3365–3371.

19 A.-V. Lupaescu, M. Iavorschi and M. Covasa, *Pharmaceutics*, 2022, **14**, 235.

20 M. Akbarian, R. Yousefi, F. Farjadian and V. N. Uversky, *Chem. Commun.*, 2020, **56**, 11354–11373.

21 B. Rosetti and S. Marchesan, *Int. J. Mol. Sci.*, 2023, **24**, 1306.

22 S. Santos, I. Torcato and M. A. R. B. Castanho, *Biopolymers*, 2012, **98**, 288–293.

23 M. Reches and E. Gazit, *Science*, 2003, **300**, 625–627.

24 N. K. Mishra, R. N. V. Krishna Deepak, R. Sankararamakrishnan and S. Verma, *J. Phys. Chem. B*, 2015, **119**, 15395–15406.

25 P. Yao, J. Zhang, S. You, W. Qi, R. Su and Z. He, *J. Mater. Chem. B*, 2020, **8**, 3076–3086.

26 J. Zhang, P. Yao, S. You, W. Qi, R. Su and Z. He, *J. Mater. Chem. B*, 2022, **10**, 7780–7788.

27 P. Ung and D. A. Winkler, *J. Med. Chem.*, 2011, **54**, 1111–1125.

28 A. M. Garcia, M. Melchionna, O. Bellotto, S. Kralj, S. Semeraro, E. Parisi, D. Iglesias, P. D'Andrea, R. De Zorzi, A. V. Vargiu and S. Marchesan, *ACS Nano*, 2021, **15**, 3015–3025.

29 M. I. Ivanova, S. A. Sievers, M. R. Sawaya, J. S. Wall and D. Eisenberg, *Proc. Natl. Acad. Sci. U. S. A.*, 2009, **106**, 18990–18995.

30 C. Thorlaksen, M. B. Neergaard, M. Groenning and V. Foderà, in *Protein Aggregation: Methods and Protocols*, ed. A. S. Cieplak, Springer US, New York, NY, 2023, pp. 297–309.

31 M. K. Siddiqi, N. Majid, P. Alam, S. Malik, A. Alam, S. Rajan, M. R. Ajmal and R. H. Khan, *Int. J. Biol. Macromol.*, 2020, **143**, 102–111.

32 B. N. Ratha, A. Ghosh, J. R. Brender, N. Gayen, H. Ilyas, C. Neeraja, K. P. Das, A. K. Mandal and A. Bhunia, *J. Biol. Chem.*, 2016, **291**, 23545–23556.

33 B. N. Ratha, R. K. Kar, S. Kalita, S. Kalita, S. Raha, A. Singha, K. Garai, B. Mandal and A. Bhunia, *Biochim. Biophys. Acta, Proteins Proteomics*, 2019, **1867**, 405–415.

34 V. Banerjee, R. K. Kar, A. Datta, K. Parthasarathi, S. Chatterjee, K. P. Das and A. Bhunia, *PLoS One*, 2013, **8**, e72318.

35 L. Nielsen, R. Khurana, A. Coats, S. Frokjaer, J. Brange, S. Vyas, V. N. Uversky and A. L. Fink, *Biochemistry*, 2001, **40**, 6036–6046.

36 N. Amdursky, Y. Erez and D. Huppert, *Acc. Chem. Res.*, 2012, **45**, 1548–1557.

37 M. Ziaunys, A. Sakalauskas and V. Smirnovas, *Biomacromolecules*, 2020, **21**, 4989–4997.

38 B. Sarmento, A. Ribeiro, F. Veiga and D. Ferreira, *Colloids Surf., B*, 2006, **53**, 193–202.

39 B. Morel, L. Varela and F. Conejero-Lara, *J. Phys. Chem. B*, 2010, **114**, 4010–4019.

40 E. Judy and N. Kishore, *Biochimie*, 2023, **207**, 20–32.

41 D. Sharma, S. Arora and J. Singh, *Int. J. Polym. Mater.*, 2020, **69**, 1054–1068.

42 W. Dzwolak, R. Ravindra, J. Lendermann and R. Winter, *Biochemistry*, 2003, **42**, 11347–11355.

43 M. Pachetti, F. D'Amico, L. Pascolo, S. Pucciarelli, A. Gessini, P. Parisse, L. Vaccari and C. Masciovecchio, *Biophys. J.*, 2021, **120**, 4575–4589.

44 D. Kurouski, J. Washington, M. Ozbil, R. Prabhakar, A. Shekhtman and I. K. Lednev, *PLoS One*, 2012, **7**, e36989.

45 S. Venturi, B. Rossi, M. Tortora, R. Torre, A. Lapini, P. Foggi, M. Paolantoni and S. Catalini, *Int. J. Biol. Macromol.*, 2023, **242**, 124621.

46 D. Kurouski, R. A. Lombardi, R. K. Dukor, I. K. Lednev and L. A. Nafie, *Chem. Commun.*, 2010, **46**, 7154–7156.

47 Z. Chi and S. A. Asher, *Biochemistry*, 1998, **37**, 2865–2872.

48 S. A. Asher, M. Ludwig and C. R. Johnson, *J. Am. Chem. Soc.*, 1986, **108**, 3186–3197.

49 E. Scarel, O. Bellotto, P. Rozhin, S. Kralj, M. Tortora, A. V. Vargiu, R. De Zorzi, B. Rossi and S. Marchesan, *Soft Matter*, 2022, **18**, 2129–2136.

50 D. A. Case, K. Belfon, I. Y. Ben-Shalom, S. R. Brozell, D. S. Cerutti, T. E. Cheatham III, V. W. D. Cruzeiro, T. A. Darden, R. E. Duke, G. Giambasu, M. K. Gilson, H. Gohlke, A. W. Goetz, R. Harris, S. Izadi, S. A. Iz-mailov, K. Kasavajhala, A. Kovalenko, R. Krasny, T. Kurtzman, T. S. Lee, S. LeGrand, P. Li, C. Lin, J. Liu, T. Luchko, R. Luo, V. Man, K. M. Merz, Y. Miao, O. Mikhailovskii, G. Monard, H. Nguyen, A. Onufriev, F. Pan, S. Pantano, R. Qi, D. R. Roe, A. Roitberg, C. Sagui, S. Schott-Verdugo, J. Shen, C. L. Simmerling, N. R. Skrynnikov, J. Smith, J. Swails, R. C. Walker, J. Wang, L. Wilson, R. M. Wolf, X. Wu, Y. Xiong, Y. Xue, D. M. York and P. A. Kollman, *AMBER 2020*, University of California, San Francisco, 2020.

51 V. I. Timofeev, R. N. Chuprov-Netochin, V. R. Samigina, V. V. Bezuglov, K. A. Miroshnikov and I. P. Kuranova, *Acta Crystallogr., Sect. F: Struct. Biol. Cryst. Commun.*, 2010, **66**, 259–263.

52 W. Humphrey, A. Dalke and K. Schulten, *J. Mol. Graphics*, 1996, **14**, 33–38.

53 C. Tian, K. Kasavajhala, K. A. A. Belfon, L. Raguette, H. Huang, A. N. Migues, J. Bickel, Y. Wang, J. Pincay, Q. Wu and C. Simmerling, *J. Chem. Theory Comput.*, 2020, **16**, 528–552.

54 O. Bellotto and S. Marchesan, in *Peptide Bionanomaterials: From Design to Application*, ed. M. A. Elsawy, Springer International Publishing, Cham, 2023, pp. 401–429, DOI: 10.1007/978-3-031-29360-3_12.